



Transport of cystine across xC^- antiporter

Maryam Ghasemitarei^{a,b,*}, Maksudbek Yusupov^b, Jamoliddin Razzokov^b, Babak Shokri^a, Annemie Bogaerts^b

^a Physics Department, Shahid Beheshti University, G.C., Evin, Tehran, 19839, Iran

^b Research Group PLASMAN, Department of Chemistry, University of Antwerp, Universiteitsplein 1, B-2610, Antwerp, Belgium

ABSTRACT

Extracellular cystine (CYC) uptake by xC^- antiporter is important for the cell viability. Especially in cancer cells, the upregulation of xC^- activity is observed, which protects these cells from intracellular oxidative stress. Hence, inhibition of the CYC uptake may eventually lead to cancer cell death. Up to now, the molecular level mechanism of the CYC uptake by xC^- antiporter has not been studied in detail.

In this study, we applied several different simulation techniques to investigate the transport of CYC through xCT , the light subunit of the xC^- antiporter, which is responsible for the CYC and glutamate translocation. Specifically, we studied the permeation of CYC across three model systems, i.e., outward facing (OF), occluded (OCC) and inward facing (IF) configurations of xCT . We also investigated the effect of mutation of Cys₃₂₇ to Ala within xCT , which was also studied experimentally in literature. This allowed us to qualitatively compare our computation results with experimental observations, and thus, to validate our simulations.

In summary, our simulations provide a molecular level mechanism of the transport of CYC across the xC^- antiporter, more specifically, which amino acid residues in the xC^- antiporter play a key role in the uptake, transport and release of CYC.

1. Introduction

The cell membrane is a complex biomolecular structure, containing mostly proteins and lipids. Among the important proteins, transporters are essential for transporting small molecules, such as amino acids and ions, which are physiologically crucial for some processes. In neurotransmission [1], the efflux of toxic compounds [2] and the regulation of glucose [3], transporters play an important role. Transporters have a range of functions and are categorized into two main groups: primary and secondary active transporters (see transporter classification database on www.tcdb.org [4]), based on whether the transport function is regulated by chemical energy or a cellular electrochemical gradient, respectively. The secondary active transporters can be grouped into three general categories [5,6], i.e., uniporter, symporter and antiporter. Uniporters mediate the transport of one molecule or ion, symporters carry two different ions or molecules in the same direction through the membrane, while antiporters transfer two different molecules (e.g., two specific amino acids) or ions through the membrane in opposite directions.

Antiporters play a key role in the preservation and proper functioning of some amino acid-dependent cellular processes, such as the energy metabolism, protein synthesis and cell protection [7]. The cells cannot sufficiently synthesize certain amino acids, and hence, for cell growth and viability, these amino acids need to be supplied from extracellular space.

One of the amino acids, vital for both normal and malignant cells, is Cys or its oxidized dimer form, cystine (CYC) [8,9]. Cys/CYC is essential for general protein biosynthesis, specifically glutathione. Since intracellular glutathione has a short half-life, CYC uptake is of high value for the cell viability [10,11].

Two distinct mechanisms for CYC uptake by normal cells have been reported [12]. 40–50% of CYC uptake is mediated by γ -glutamyl transpeptidase, which is located on the outer surface of the cell membrane and part of the γ -glutamyl cycle. The other 50–60% is thought to be provided by xC^- antiporter, which is a so-called electroneutral, anionic CYC-Glu transporter [12,13]. Indeed, the anionic forms of extracellular CYC and intracellular Glu exchange with a stoichiometry of 1:1 [7,14], and thus, no net charge is transported across the membrane.

The xC^- antiporter has two important functions. Firstly, it assists with extracellular CYC uptake, increasing the intracellular level of glutathione, which helps to protect cells from oxidative stress. Secondly, it helps to balance extracellular CYC and Cys, which is important for proliferation of T cells [15]. T cells (or T lymphocytes) play a central role in cell-mediated immunity. After passing through the xC^- antiporter, CYC is reduced to Cys and is incorporated into the glutathione structure. Glutathione is composed of three amino acids, i.e., Glu, Cys and Gly. These three amino acids play an important role in cell protection from drug-induced oxidative stress [16]. CYC uptake by xC^- antiporter can occur more frequently in two cases, i.e., a) as a result of a low level of intracellular CYC compared to the extracellular level and b)

* Corresponding author. Physics Department, Shahid Beheshti University, G.C., Evin, Tehran, 19839, Iran.

E-mail addresses: mar_ghasemi@sbu.ac.ir, Maryam.Ghasemitarei@uantwerpen.be (M. Ghasemitarei).

because of the high concentration of intracellular Glu. The latter can take place due to the transport of Glu by the Ala-Ser-Cys (ASC) transporter into the cell [12].

The xC^- antiporter plays a critical role in many diseases, especially in cancer [17–19]. It has been reported that some cancer cells such as leukemia and lymphoma, are not able to synthesize Cys [20,21]. This could be caused by the lack of γ -cystathionase, which is the enzyme that breaks down cystathionine to Cys, α -ketobutyrate, and ammonia. As a result, extracellular CYC uptake by e.g., the xC^- antiporter becomes important for cancer cell growth and viability. Because lymphoid cells cannot synthesize endogenous Cys, and CYC uptake in extracellular acidic pH conditions of cancer cells is depleted, they generally cannot have high CYC uptake. Therefore, upregulation of xC^- activity in cancer cells is observed, which preserves the antioxidant defense.

Thus, cancer cells can uptake CYC directly by expressing the xC^- antiporters. As a consequence, the importance of these transporters could make them a cancer therapy target [22–24]. CYC uptake could be interrupted by inhibiting these transporters, which would reduce glutathione synthesis, and thus, the cellular protection from oxidative stress, eventually leading to reduced viability and growth in cancer cells [25]. This antiporter also contributes to cancer cell drug resistance: CYC uptake enhances the biosynthesis of glutathione which mediates the cellular detoxification of drugs. As a result, the inhibition of the xC^- antiporter, and consequently, reduction of glutathione, not only inhibits cancer cell growth [26], but also reduces drug resistance [12,27,28].

Previous studies have shown that the viability of lymphoma and leukemia cells critically depends on the extracellular CYC/Cys concentration, and that the depletion of this amino acid in circulation can provide a useful therapeutic approach for these malignancies [12,24,29].

Structurally, the xC^- antiporter is a member of the heteromeric amino acid transporter (HAT) family. These transporters are made of a light subunit that belongs to the LAT family (i.e., the family of L amino acid transporters), and a heavy subunit coupled to the light subunit by a disulfide bridge [30,31]. The LAT family has 12 transmembrane (TM) domains and is non-N-glycosylated (see Fig. 1(A)) [6,32]. The light and heavy subunits have different functions: the heavy subunit is involved in maintaining the entire antiporter structure in the plasma membrane, while the light subunit is responsible for the transport [30,31].

Studying the three-dimensional (3D) structure of antiporters is important for conformational analysis, ion free energy calculation, substrate binding and the evaluation of the light and heavy subunit functions in the amino acid transport cycle. One of the most powerful tools for identification of the atomic 3D structure of membrane transporter proteins is x-ray crystallography [33]. Unfortunately, the structural investigation of HATs at the atomic scale is limited to the study of prokaryotic homologues of the light subunit [5] and of the ectodomain (i.e., the domain that extends into the extracellular space) of the heavy subunit. The lack of crystal structures of the LAT family, including that of xCT (i.e., the light subunit of the xC^- antiporter, see Fig. 1(A)), makes it difficult to determine the exact amino acid residues [34] which play an essential role in the translocation mechanism of these transporters. Homology modeling [35] and simulation techniques, such as molecular dynamics (MD) [36], could contribute to a better understanding of this mechanism.

Three different conformations, i.e., outward facing (OF), occluded (OCC) and inward facing (IF) have been reported for e.g., AdiC [37], GadC [38] and xCT, based on the crystal structure of these proteins.

First, CYC binds to an OF conformation (see Fig. 1(B)). Subsequently, during the closure of the outer side and the transition to an IF state, the opposite side of the membrane becomes available to release the CYC to the cell interior. During the transport of CYC and the transition from the OF to the IF state, the binding site of xCT becomes partially or completely occluded, i.e., OCC.

The structure and transport mechanism of so-called ApcT [37] transporter (which is another transporter of the same family as xCT)

was first investigated by Shaffer et al. in 2009 [37]. They reported that tyrosine at position 97 (Tyr₉₇) of TM3 is part of the possible substrate binding site. The authors also suggested that the hypothetical substrate binding site of xCT should be arginine at position 135 (Arg₁₃₅), which is equivalent to Tyr₉₇ (i.e., at the same position as Tyr₉₇ in the amino acid sequence) of the ApcT transporter. The first homology model for xCT was constructed by Janaschii, using the crystal structure of ApcT (PDB ID: 3GIA) [17]. In 2010 Gao et al. determined the crystal structure of Arg/Agmatine transporter (AdiC) (PDB ID: 3L1L) [39]. However, the lack of details on the structural changes, such as transitions from OF to IF state, as well as the substrate binding/release site, explains the need for powerful computational tools to investigate these important processes.

MD simulation techniques are strong tools for understanding and studying the dynamics and mechanics of all related steps [40]. They are able to find conformational transitions in large-scale proteins, such as antiporters. Recently, non-equilibrium MD methods, such as targeted MD (TMD) [41], steered MD (SMD) [42], accelerated MD [43] and metadynamics [44], as well as umbrella sampling (US) [45] have been used frequently to investigate the conformational transitions in various transporters [40,46,47].

In the present study, we modeled the xCT subunit of xC^- antiporter based on two different states of AdiC and one state of GLU/GABA (GadC) transporters, by using homology modeling. We simulated the extracellular to intracellular transition of CYC through xCT, applying a combination of TMD, SMD and classical MD simulations. We used SMD to pull CYC into the OF state of the xCT, in order to find xCT's most probable binding position. Furthermore, we used TMD to change the conformation of xCT from OF to OCC, as well as from OCC to IF structure. Prior to each TMD simulation, we performed classical MD simulations to relax the systems. We also found out the amino acids of xCT which play an important role in CYC binding, such as Arg₁₃₅ and Arg₃₉₆. Moreover, we performed US simulations to validate our model predictions, through qualitative comparison of the computational results with experimental observations [48].

2. Computational details

2.1. Choosing the model systems

In our simulations we focused on the OF, OCC and IF conformations of xCT, i.e., the light subunit of xC^- antiporter, since the xCT is responsible for transporting amino acids. Specifically, we studied the extracellular to intracellular translocation of CYC across these model systems.

The 3D structure of xCT is not available in the protein data bank [49]. To study its structure and to find out its substrate binding site, we modeled this structure by using its protein sequence. Hence, to make the best model, we applied homology modeling using similar structures (or templates) to xCT from the protein data bank. Based on the Sander and Schneider alignment algorithm [50], for proteins with residue numbers in the range of 10–80, the threshold for similarity of target and template can be represented by the formula:

$$t(L) = 290.15L^{-0.562}$$

where L is the number of aligned residues. For proteins with more than 80 residues ($L > 80$), as in our case, the similarity threshold should be around 25%. The templates that were selected for OF and OCC conformations have enough similarities with the xCT subunit. Specifically, the OF open face of AdiC (PDB ID: 30B6 [51]) with similarity 24.83% was chosen as a template for the OF conformation of xCT. For the OCC conformation of xCT, the occluded face of AdiC (PDB ID: 3L1L [39]) with similarity 24.50% was applied as a template. Unfortunately, there is no template structure available with a high (i.e., ~25%) similarity to the IF conformation of xCT. Therefore, we used the IF open

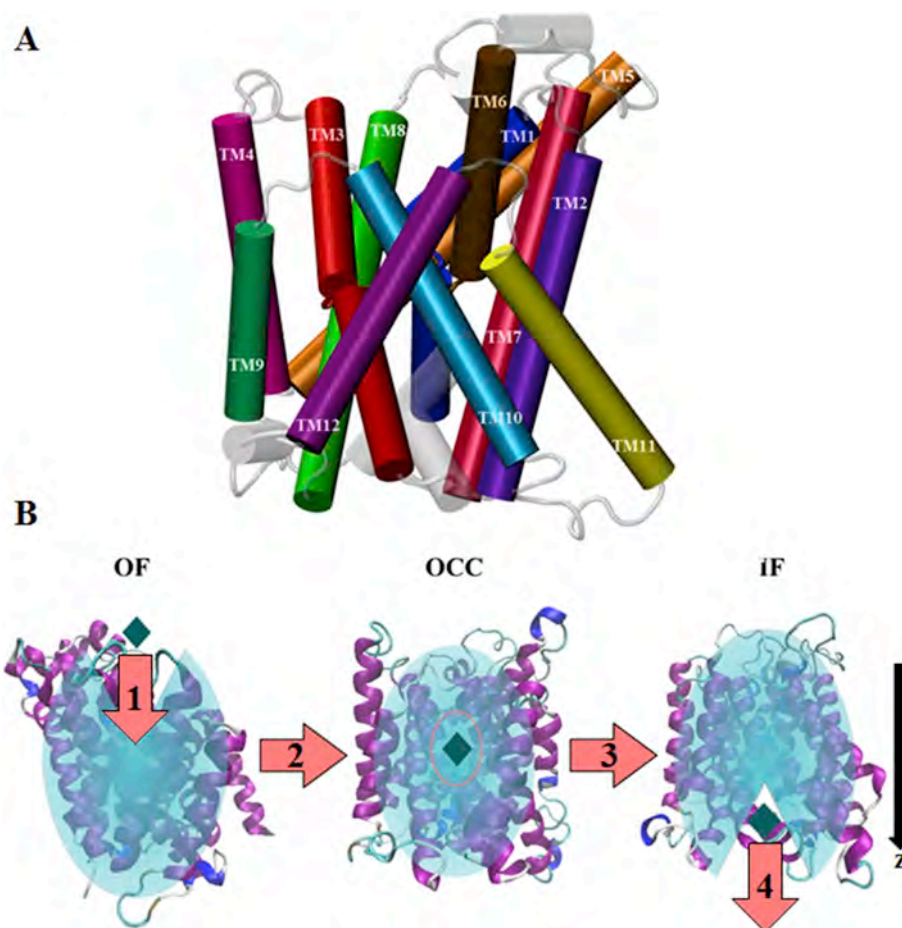


Fig. 1. (A) The 12 transmembrane (TM) domains of xCT, i.e., the light subunit of the xCT^- antiporter. (B) Schematic representation of the three different states of the xCT subunit of the xCT^- antiporter, i.e., OF, OCC and IF. CYC is presented as green diamond. An arrow indicates the transition of CYC from the extracellular to the intracellular part of the membrane. (For interpretation of the references to color in this figure legend, the reader is referred to the Web version of this article.)

conformation of GadC (PDB ID: 4DJ1 [52]) as a template, which has the highest available similarity to the xCT subunit, i.e., 17.41% (see also the alignment between the amino acid residues of xCT (i.e., its three conformations OF, OCC and IF) and template structures in Fig. S1).

2.2. Preparation of the model systems

The protein sequence (FASTA) of human xCT [30,53] subunit was extracted from the NCBI website (<https://www.ncbi.nlm.nih.gov/>). The SWISS-MODEL server [54] was used to find the best templates and to make the model structures. The orientation of the model proteins into the lipid bilayer surrounding them was determined by the OPM [55] database (<http://opm.phar.umich.edu/>). 1-palmitoyl-2-oleoyl-*sn*-glycero-3-phosphocholine (POPC) molecules were used to build the lipid bilayer and ions and water molecules were added by applying the CHARMM GUI [56,57] web server (<http://www.charmm-gui.org>). Three different kinds of CYC are found in the extracellular milieu, i.e., CYC with two carboxylate groups and two protonated amino groups (CYC-I), CYC with two carboxylate groups and one protonated and one neutral amino group (CYC-II) and CYC with two carboxylate groups and two neutral amino groups (CYC-III). Based on literature, CYC-II is the one that can pass through xCT^- antiporters [58]. Therefore, we used CYC-II (which is negatively charged) to study its transport through xCT in our simulations. The force field parameters for bonded and non-bonded interactions of CYC-II are not available in force field databases. Hence, similar to the procedure used by van der Spoel et al. [59], we employed Gaussian16 [60] and the CHARMM general force field (CGenFF) [61] (see <https://cgenff.parachem.org>), to obtain the force

field parameters needed for CYC-II. Specifically, applying the Gaussian16 program, we used the DFT method with the standard 6-311G* basis set to optimize CYC-II and generate its partial charges. Afterwards, using the output from Gaussian16, we applied the CGenFF program to obtain the topology files that contain the force field parameters of CYC-II. These parameters are compatible with the charmm36 force field used for the rest of the system.

2.3. Validation of the model systems

The ERRAT, Verify3D and Procheck programs were used to analyze the quality of the OF, OCC and IF models (see below), applying the web server <http://servicesn.mbi.ucla.edu/SAVES/> [62]. Moreover, the protein structure quality score (PSQS) was used to measure the quality of the model structures, by describing the interactions between residue pairs as well as between single residues and solvent (see <http://www1.jcsg.org/psqs/>). The Verify3D program was used to determine the compatibility between the 3D structure of the model and its sequence of amino acids (1D). The ERRAT program was applied to analyze the statistics of non-bonded interactions between side chains, lipids and solvents. The Procheck program compares residues using the geometry of both residues and structure (i.e., the standard Ramachandran plot). It checks the dihedral angles ψ against ϕ of the residue backbone of the protein structures.

The topology model of the 12 TM domains of the xCT subunit was obtained experimentally by Gasol et al. [53]. Based on this model, we determined the amino acid residues that form the 12 TM domains (see Fig. 2(A)). Fig. 2(B) represents these residues in purple, while the other

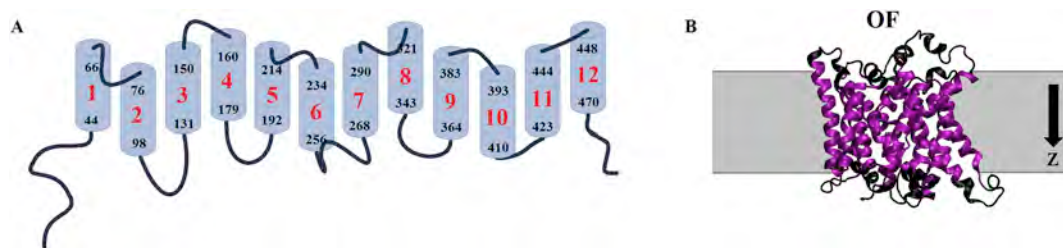


Fig. 2. (A) Schematic representation of the 12 TM domains of the xCT subunit, with the residue numbers in each of them. (B) The residues that form the 12 TM domains are shown in purple color, while the rest are in black color, for the OF structure. The same applies to the IF and OCC structures. The membrane (region) is simply represented by the gray box. The direction of the z-axis is shown with black arrow. (For interpretation of the references to color in this figure legend, the reader is referred to the Web version of this article.)

residues, which are not in the TM domains, are shown in black.

2.4. MD simulation protocols

Applying the NAMD 2.12 program [63], the MD simulations were carried out in the isothermal-isobaric (NPT) ensemble at 310 K and 1 atm. The CHARMM36 [64,65] force field was used to describe the model systems, including the proteins (i.e., OF, OCC, IF), phospholipids, ions, water and CYC. Prior to the MD simulations, the systems were energy minimized using the steepest descent algorithm. The Verlet list scheme was applied with a 12 Å cutoff for both the electrostatic and van der Waals interactions. The Particle-mesh Ewald method was applied to calculate long-range electrostatic interactions. We applied the Nose-Hoover thermostat [66] in combination with a coupling constant of 1 ps and the semi-isotropic Parrinello-Rahman barostat [67] with a compressibility of $4.5 \times 10^{-5} \text{ bar}^{-1}$ and a coupling constant of 5 ps. In all systems, the net positive charge was neutralized by adding chlorine ions to the water layer. Each system was composed of 202 phospholipids, the protein (either OF, OCC, or IF) and 15000 water molecules. All simulations were carried out with periodic boundary conditions in a box with dimensions of $\approx 105 \times 105 \times 95 \text{ Å}^3$ and a time step of 2 fs was used in all simulations.

After equilibration of all three systems (which we call simply OF, OCC and IF structures) for 500 ns (see Fig. S2), the HOLE program [68] was used to compute the radius of the model systems' cavity along the z direction, i.e., the direction passing through the pore channel. In other words, the HOLE program was used to analyze and visualize the pore dimension through the molecular structure of the protein channels for OF, OCC and IF structure. This program proceeds along the plane perpendicular to the channel vector and finds the largest sphere without overlapping with the van der Waals surface of any atom. Subsequently, a small displacement is taken in the direction of the channel vector and this process is repeated for the next plane as well. In this study, the funnel radius was computed using more than 50 configurations, extracted from the last 50 ns of the MD trajectories of the equilibration process.

SMD was used to pull CYC towards the OF structure along the z direction. This procedure was repeated 5 times, employing different initial configurations extracted with a 10 ns interval from the last 50 ns of the MD trajectories. Each SMD simulation lasted for 10 ns. This is done in order to define the precise position of CYC at the substrate binding site, as the positions of the side chains at the substrate binding site in these configurations might differ due to the fluctuations during the MD simulation and this might affect the accuracy of the results. Using the results of the SMD simulations, the more precise position of CYC at the substrate binding site was defined. After pulling was completed, the system was relaxed for 6 ns, using conventional MD simulations.

Subsequently, TMD simulations were carried out to transport CYC across the xCT system, i.e., for permeation of CYC into the OF configuration, staying in the OCC structure and moving out from the IF

conformation (see above in Fig. 1(B)). Initially, 10 ns TMD was performed to guide CYC into the OF structure (step 1 in Fig. 1(B)), applying an elastic constant of $2500 \text{ kcal. mol}^{-1} \text{ Å}^{-2}$. This transportation was continued up to the target position of CYC, which was determined by the results of the SMD simulations. After that, the transition of the structure from the OF to the OCC state was performed, applying TMD for again 10 ns (step 2 in Fig. 1(B)). In this simulation, the backbone of the equilibrated OCC conformation was used as the target structure. In other words, all atoms of the OF structure were guided towards a final (i.e., the OCC) structure by means of steering forces. Subsequently, the transition from the OCC to the IF state was carried out again by using TMD for 10 ns (step 3 in Fig. 1(B)). Finally, CYC was moved out from the IF structure using another 10 ns TMD (step 4 in Fig. 1(B)). This entire procedure was repeated using the last conformations of the 5 relaxed systems. As in the case of SMD, all TMD simulations were followed by 6 ns conventional MD simulations to relax the system.

We used the NAMD Energy plugin of the VMD software [69] to compute the non-bonded energy between CYC and each amino acid of the OF, OCC and IF structures, located at a distance less than 12 Å from CYC. Note that the NAMD Energy plugin calculates the energy of either one or two selected structures (or molecules); if only one structure is selected, the internal and interaction energies of that structure are calculated, whereas if two different structures are selected, only the interaction energies between these structures are calculated.

2.5. US simulations

It was found experimentally [48] that the mutation of Cys₃₂₇ to Ala within xCT makes the CYC uptake into cells more difficult. To check this, as well as to validate our simulation results, we performed US simulations applying the GROMACS 5.0.4 package [70,71]. As model systems in our US simulations, we used the native and modified (i.e., Cys₃₂₇ to Ala) structures of the OF configuration, as well as the native structures of the OCC and IF structures. For the mutation of Cys₃₂₇ to Ala, we used the free PYMOL version 1.4.1-3 [72].

Prior to the US simulations, the HOLE program was used to find the starting and end positions of CYC for pulling into the systems. The points presented in Fig. 3 (i.e., a, b, c, d, e and f) indicate these positions of CYC in the OF, OCC and IF structures, which were used in the US simulations. For instance, in the OF structure, the initial position of CYC (see point a in Fig. 3) was in the extracellular milieu, i.e., at -3.9 nm distance from the center of mass (COM) of the protein (i.e., close to the aperture of the OF channel). The harmonic biasing force was applied to pull CYC against the OF's COM with a force constant of $1000 \text{ kJ.mol}^{-1} \text{ nm}^{-2}$ and a pulling rate of 0.01 nm.ps^{-1} . The pulling was performed in the periodic direction geometry along the z direction for 1100 ps in the OF and IF system and 600 ps in the OCC system. For each energy profile, 98 windows were extracted for both native and modified form of the OF structure. The same procedure was applied for the US simulation of the OCC and IF structures, but the number of umbrella windows was somewhat different, i.e., 46 windows were extracted for

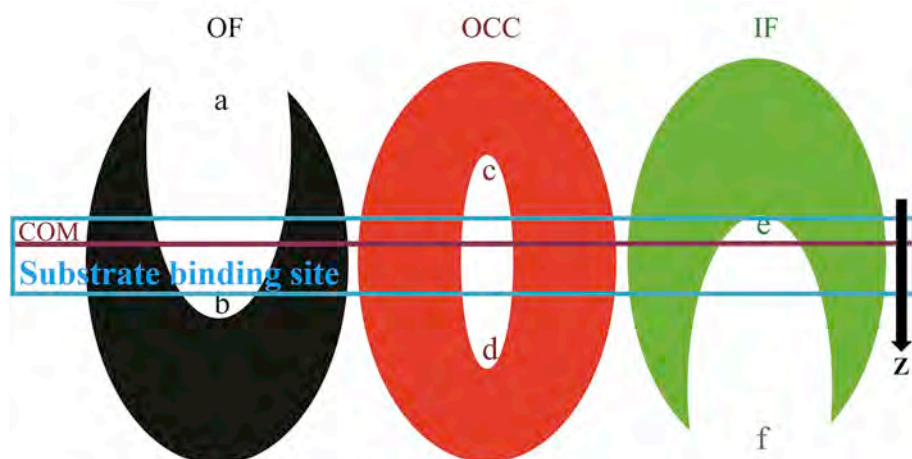


Fig. 3. Initial and final positions of CYC used in the US simulations for the OF (a and b), OCC (c and d) and IF (e and f) states of xCT. The approximate position of the COM and the substrate binding site of all structures are indicated by the red line and blue rectangle, respectively. (For interpretation of the references to color in this figure legend, the reader is referred to the Web version of this article.)

the OCC and 75 for the IF structures. The windows in these simulations were all separated by ≤ 0.1 nm. Note that in this manner, the sampling windows spanned the entire system ranging from -3.9 till $+3.9$ along the z direction, where both minimum and maximum positions corresponded to intracellular and extracellular water phases, respectively. Each US simulation lasted for 20 ns, where the last 15 ns was used for construction of the free energy profiles. Each free energy profile was calculated using a periodic version of the weighted histogram analysis method (WHAM) [73]. The final free energy profile was obtained over four free energy profiles for each system. In total, $98 \times 4 + 46 \times 4 + 75 \times 4 = 876$ US simulations were performed to obtain the free energy profiles.

3. Result and discussion

3.1. Quality of the chosen model structures

As mentioned in section 2.3, to validate the used model systems we applied different programs (i.e., ERRAT, Verify3D, Procheck (see <http://nihserver.mbi.ucla.edu/SAVS/>) and PSQS (see <http://www1.jcsg.org/psqs>)). Table 1 shows the quality scores of the OF, OCC and IF model systems. The PSQS of the models and templates had the same values, whereas the Verify3D score of the models was less than that for the templates. On the other hand, the ERRAT and ProCheck analyses showed good compatibility between the models and templates (see Table 1).

The results of the Ramachandran plot of the conformations of the three model systems are given in Table 2. None of the amino acids in the OCC conformation was in the outlier region. For the OF and IF configurations, the percentage of the outlier region was less than 2%, which means that less than 6 amino acids were in this region.

These analyses of the quality of the model systems, using different programs, showed that the chosen model structures were adequate. To support this conclusion we further calculated the funnel radii of the model structures in the following section.

Table 1
Quality scores of the OF, OCC and IF model systems.

| Structure | Verify3D (%) | PSQS | ERRAT (%) | ProCheck (%) |
|-----------------|--------------|------|-----------|--------------|
| OF (model) | 57.44 | -0.3 | 91.57 | 97.3 |
| 3OB6 (template) | 80.23 | -0.3 | 98.81 | 92.8 |
| OCC (model) | 58.51 | -0.3 | 80.66 | 96.8 |
| 3L1L (template) | 81.56 | -0.3 | 97.56 | 92.4 |
| IF (model) | 50.63 | -0.3 | 77.07 | 94.3 |
| 4DJ1 (template) | 86.21 | -0.3 | 80.33 | 77.8 |

Table 2
Ramachandran plot results of the OF, OCC and IF conformations.

| Structures | Favored region (%) | Allowed regions (%) | Outlier region (%) |
|------------|--------------------|---------------------|--------------------|
| OF model | 97.3 | 1.7 | 1.0 |
| OCC model | 96.8 | 3.2 | 0.0 |
| IF model | 94.3 | 4.0 | 1.7 |

3.2. Funnel radii of the OF, OCC and IF structures

We calculated the funnel radii of the OF, OCC and IF structures, in order to examine whether the chosen model systems are sufficient to describe their channels.

Fig. 4 shows the profiles of the average funnel radii as a function of position along the transporter axis (i.e., z direction), calculated for the OF, OCC and IF structures. The OF state of the xCT subunit was open to the extracellular milieu and access to the substrate binding site was only available from the outside of the cell (see black curve in Fig. 4). Moreover, the structure was completely closed at around $z = 5$ Å, and water molecules were unable to pass through the protein, showing no access from the intracellular fluid. On the other hand, the OCC state was partially closed (cf. the initial and final funnel radii of the OCC structure, red curve in Fig. 4), having a cavity in the middle of the structure,

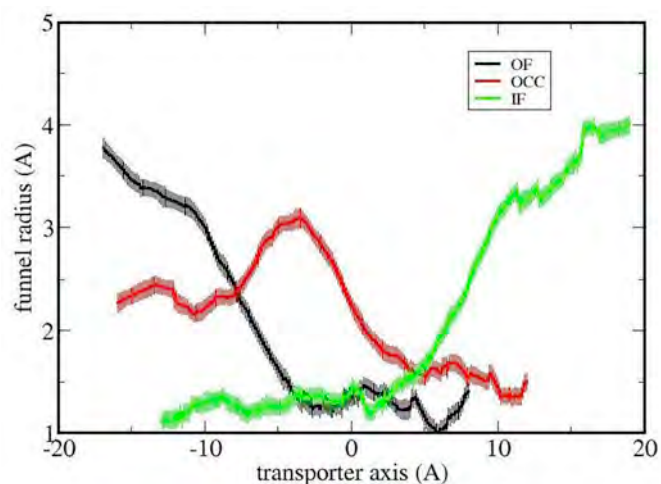


Fig. 4. Funnel radii versus position along the transporter axis, calculated for the OF (black), OCC (red) and IF (green) structures. The radii are averaged over the last 50 ns of the equilibration runs. (For interpretation of the references to color in this figure legend, the reader is referred to the Web version of this article.)

which let CYC move freely. It was still closed to the intracellular milieu and water molecules could not enter from this site due to the small size of the channel (see funnel radius at $z = 5\text{--}11 \text{ \AA}$). Finally, the IF structure was completely closed for the extracellular milieu, but it was open to the intracellular fluid. Hence, the substrate binding site was accessible to the intracellular fluid, which allowed CYC to move towards the inside of the cell (see green curve in Fig. 4). These results on the funnel radii showed again that the chosen model systems were adequate and that they appropriately described their channels.

3.3. Transport of CYC across xCT

As mentioned in section 2.4, we used SMD, TMD and subsequent conventional MD simulations to study the transport of CYC through xCT, more specifically through the OF, OCC and IF structures. SMD was used to pull CYC towards the OF state along the z direction, in order to find its most probable position in the substrate binding site of the OF structure. Subsequently, we performed TMD to clarify whether this position is energetically favorable. Further, we again applied TMD to transform the OF to the OCC structure, as well as from the OCC to the IF structure, and we analyzed the substrate binding site through examining the residues surrounding CYC and calculating their interaction energies with CYC. Conventional MD was used between each process to relax the systems.

3.3.1. Determination of the substrate binding site in the of conformation

The results of SMD are summarized in Fig. 5. As is clear from Fig. 5(B), CYC was trapped between two Arg residues with positive charges (i.e., Arg₁₃₅ and Arg₃₉₆), which form strong electrostatic interactions with the negatively charged CYC substrate. Fig. 5(A) shows the time evolution of the average distance between the alpha carbons of CYC and these two Arg residues. CYC could not escape from the attraction of these residues and the distance between them remained constant (i.e., less than 5 Å) after 5 ns, even if the pulling was still continued. Thus, these Arg residues play an important role as CYC binding sites.

To verify this, we subsequently performed TMD (and conventional MD) simulations. Specifically, we calculated the non-bonded energy between CYC and all amino acids of the OF structure, located at a distance less than 12 Å from CYC, applying the NAMM Energy plugin. Table 3 illustrates the average non-bonded energies between CYC and the seven amino acids with most favorable interactions, i.e., with the highest absolute non-bonded energies with CYC. This table also presents the non-bonded energy of CYC with all aromatic residues (i.e., Phe, Tyr and Trp, if any), located within 12 Å around CYC. We included the aromatic residues, as they could form a cation- π interaction, i.e.,

Table 3

Non-bonded energies of CYC with the seven amino acids with most favorable interactions, as well as with the aromatic residues of the OF structure, located within 12 Å from CYC, i.e., in the substrate binding site.

| Amino acids | Non-bonded energy (kJ/mol) |
|--------------------|----------------------------|
| Arg ₁₃₅ | -193.1 ± 1.9 |
| Arg ₃₉₆ | -138.8 ± 0.6 |
| Arg ₁₂₆ | -130.1 ± 0.7 |
| Lys ₁₉₈ | -38.5 ± 0.4 |
| Glu ₁₃₀ | 237.9 ± 0.9 |
| Arg ₃₄₀ | -48.2 ± 0.2 |
| Glu ₂₅₇ | 24.9 ± 0.2 |
| Aromatic | -29.5 ± 0.8 |

interaction between the benzene groups of the aromatic residues and the protonated amino group of CYC. Note that there were also other residues which might interact with CYC, but their relative non-bonded energies were lower than those shown in Table 3. However, the energies of these residues were considered when calculating the total non-bonded energy of CYC (see below). As is clear in Table 3, Arg₁₃₅ of TM3, Arg₃₉₆ of TM9 and Arg₁₂₆ between TM2 and TM3 had strong attractive interactions with CYC. Indeed, the positively charged guanidino groups of these amino acids formed a strong electrostatic attraction with the carboxylate groups of CYC (see e.g., Fig. 5(B)). On the other hand, Glu₁₃₀ exhibited a strong repulsive interaction, since it also had a negatively charged carboxylate group, like CYC. Other amino acids (i.e., Lys₁₉₈, Arg₃₄₀ and Glu₂₅₇) and the aromatic residues did not form strong interactions. In general, the total non-bonded energy between CYC and all residues found within 12 Å from CYC, was equal to $-53.68 \pm 0.67 \text{ kJ.mol}^{-1}$, which indicated that CYC had overall a strong attractive interaction with the substrate binding site. Note that a lot of other amino acid residues contributed to this total energy, which explains why this value is not the same as the sum of the values defined in Table 3.

3.3.2. Occlusion of the of structure

The transition from the OF to the OCC structure led to a change in positions of the amino acid residues, including those located in the substrate binding site. Analysis of the calculated average root mean square deviation (RMSD) of each residue over time showed that the residues in TM2, TM9, TM10, TM11 and TM12 had the largest change in position during this transition (see Fig. S3(A)), exhibiting slight movements of the residues in TM4 and TM6, which was enough to affect the local and total conformational changes. Table 4 shows the average non-bonded energies of CYC with the seven amino acids with

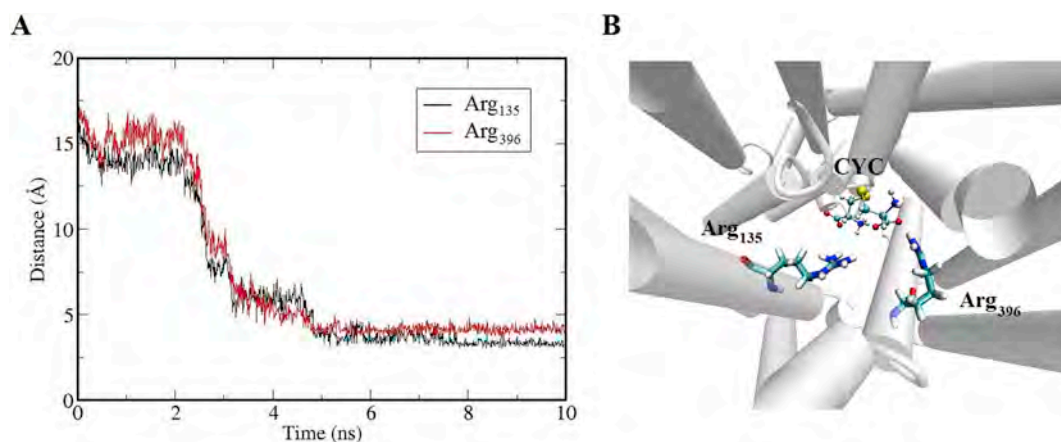


Fig. 5. (A) Average distances between CYC and two Arg residues (i.e., Arg₁₃₅ and Arg₃₉₆) positioned at the substrate binding site. (B) Position of CYC in the vicinity of the positively charged Arg₁₃₅ and Arg₃₉₆. These residues strongly interact with the negatively charged CYC and do not let it move into the protein.

Table 4

Non-bonded energies of CYC with the seven amino acids with most favorable interactions, as well as with the aromatic residues of the OCC structure, located within 12 Å from CYC, i.e., in the substrate binding site.

| Amino acids | Non-bonded energy (kJ/mol) |
|--------------------|----------------------------|
| Arg ₁₃₅ | −138.8 ± 0.6 |
| Arg ₃₉₆ | −24.5 ± 0.1 |
| Arg ₁₂₆ | −14.3 ± 0.1 |
| Lys ₁₉₈ | −62.3 ± 0.9 |
| Glu ₁₃₀ | 49.6 ± 0.4 |
| Arg ₃₄₀ | −50.2 ± 0.5 |
| Asp ₃₈₄ | 71.9 ± 0.5 |
| Aromatic | −60.1 ± 0.8 |

most favorable interactions and with the aromatic residues (see Table 3 in previous section), for the OCC structure. The attractive energy between CYC and Arg₃₉₆ reduced significantly, due to an increasing distance between them. Moreover, the energy increased between CYC and Lys₁₉₈ of TM4 (cf. Tables 3 and 4) because of the movement of the residues in the TM4 domain (see above) and shortening of the distance between these residues and CYC. Furthermore, Arg₁₃₅ of TM3 was still the most attractively interacting amino acid with CYC (see Table 4 and Fig. S3 for more details).

Interestingly, the repulsive energy between CYC and Glu₁₃₀ also reduced (cf. Tables 3 and 4) due to an increasing distance between them. In addition, Asp₃₈₄ now interacted with CYC instead of Glu₂₅₇ found in the OF structure (cf. Tables 3 and 4). Overall, the total non-bonded energy between CYC and all residues located within a distance of 12 Å was found to be -55.23 ± 0.12 kJ.mol⁻¹, which was slightly more negative than in the case of the OF structure. This means that CYC still experienced an attractive interaction at the substrate binding site of the OCC structure, with even a slightly higher energy.

3.3.3. Transition from the OCC to the IF structure

Study of the transition of the OCC to the IF structure is essential, as it allows to define the residues at the substrate binding site before release of CYC, and their interaction energy with CYC explains whether CYC was able to be released into the intracellular fluid. Analysis of the RMSD of each amino acid residue over time showed that the residues of TM5 and TM8 had the largest displacements during this transition (see Fig. S3 (B)). Moreover, the slight movements of the amino acid residues of TM1, TM4, TM9, TM10, TM11 and TM12 were enough to affect the conformational changes. These movements resulted in the release of CYC into the intracellular fluid. Table 5 summarizes the results of these movements. It was clear that in the IF conformation, Lys₁₉₈ played an important role in the substrate binding site; its strong interaction with CYC was a result of the TM1 and TM4 movements. We clearly saw a further decrease of the attractive energy of Arg₁₃₅ compared to OF and OCC structures (cf. Tables 3–5). This was due to a strong interaction of

Table 5

Non-bonded energies of CYC with the seven amino acids with most favorable interactions, as well as with the aromatic residues of the IF structure, located within 12 Å from CYC, i.e., in the substrate binding site.

| Amino acids | Non-bonded energy (kJ/mol) |
|--------------------|----------------------------|
| Arg ₁₃₅ | −85.7 ± 0.6 |
| Arg ₃₉₆ | −56.6 ± 0.5 |
| Arg ₁₄₈ | −34.9 ± 0.2 |
| Lys ₁₉₈ | −337.7 ± 2.5 |
| Glu ₁₃₀ | 44.1 ± 0.9 |
| Arg ₃₄₀ | −45.8 ± 0.2 |
| Lys ₆₇ | −28.3 ± 0.1 |
| Aromatic | −79.2 ± 0.9 |

CYC with Lys₁₉₈ positioned closer to the aperture, which brought CYC closer to the intracellular fluid, and thus further away from Arg₁₃₅. The total non-bonded energy between CYC and all amino acid residues within a distance of 12 Å was equal to -42.72 ± 0.50 kJ.mol⁻¹. This energy was less negative than for the OF and OCC structures, which indicated that CYC could more easily be released into the intracellular fluid.

3.4. US simulations

To support the results obtained in section 3.3, we performed US simulations in order to calculate the free energy profiles for transport of CYC through the OF, OCC and IF structures. Fig. 6 illustrates the free energy profiles of CYC across the native OF, OCC and IF structures. Note that these free energy profiles were calculated with respect to the water phase in the cases of OF and IF (see Fig. 6(A)), whereas in the OCC case the minimum energy of CYC was chosen as a reference state (Fig. 6(B)). The latter was done, since the water phase cannot be used as a reference state. Thus, the energy values obtained for OCC cannot be compared with the energy values of OF and IF (cf. Fig. 6(A) and (B)). The obtained free energy minima of CYC indicated the substrate binding site, which is shown within the blue rectangle. These free energy minima were -33.09 ± 4.16 kJ mol⁻¹ and -17.14 ± 2.38 kJ mol⁻¹, for the OF and IF structures, respectively. The free energy minima were located at -0.22 nm, 0.09 nm and 0.52 nm from the COMs of the OF, OCC and IF structures, respectively. This indicated that the position of the substrate binding site changed during the transport and it moved towards the intracellular fluid. These alterations in the position of the substrate binding site, as well as in the amino acid residues surrounding CYC at the binding site (see previous sections), guided CYC towards the intracellular fluid. This was also obvious from the free energy minimum of CYC, which increased in the case of the IF conformation, indicating that a lower energy was required to release CYC from the antiporter.

Finally, we studied the effect of a mutation in the xCT antiporter on the permeation of CYC, and more specifically the mutation of Cys₃₂₇ to Ala, which was reported in literature to make the CYC uptake into cells more difficult [48]. This study allowed us to qualitatively check the validity of our simulations, and to elucidate the reason for this effect at the molecular level. The result is shown in Fig. 7, where the free energy profiles of CYC for the native and mutated OF structures are compared.

The mutation of Cys₃₂₇ to Ala in the OF structure created an extra barrier of 32.4 kJmol⁻¹, in the free energy profile (see red curve in Fig. 7), making the CYC penetration to the substrate binding site more difficult. Furthermore, due to conformational changes in the mutated OF structure, the free energy profiles of CYC translocation had its minimum energy at around -1.5 nm, i.e., close to the extracellular region, making its motion more difficult towards the inside of the OF structure. This was in qualitative agreement with literature, as it was found that the mutation of Cys₃₂₇ of TM8 to Ala decreased the CYC uptake by the xC⁻ antiporter [48]. Thus, our computation results support the experimental observations, which could serve as a qualitative validation of our simulations.

Based on literature, Cys₃₂₇ of TM8 plays a critical role in CYC transporting [48]. The mutation of this residue to Ala could lead to depletion of CYC transport through the xC⁻ antiporter. Indeed, Ala, a nonpolar and aliphatic amino acid, contains a methyl group as a side chain [74]. Hence, it was hardly involved in the transport function of xC⁻, explaining why CYC translocation became indeed more difficult.

4. Conclusions

We studied the transport of CYC across the xCT subunit of the xC⁻ antiporter. This might be important as future cancer therapy target. Indeed, in cancer cells an enhanced transport of CYC across the xC⁻ antiporter is observed, and this protects the cancer cells from intracellular oxidative stress. If the CYC uptake can be inhibited, this

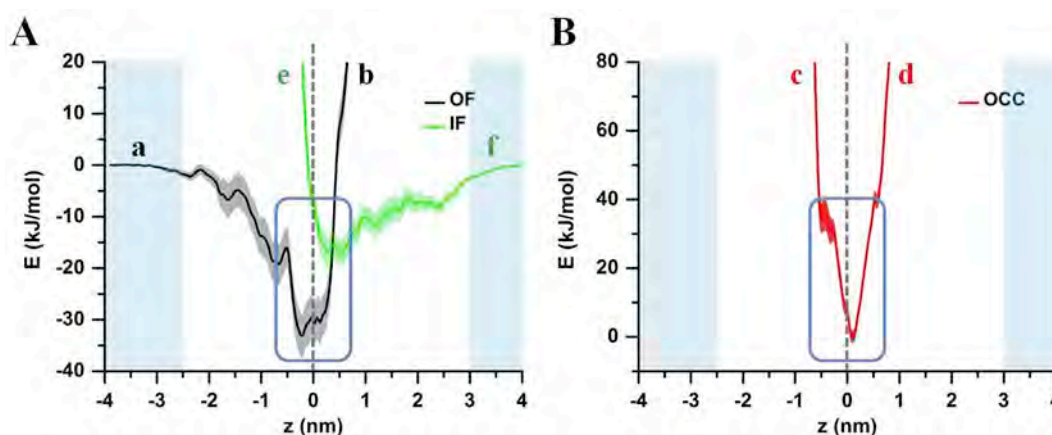


Fig. 6. Free energy profiles for the translocation of CYC across the (A) OF and IF and (B) OCC states of xCT. The positions of the COM and the substrate binding site are indicated by the gray dashed line and blue rectangle, respectively. The letters a-f refer to the positions in Fig. 3. (For interpretation of the references to color in this figure legend, the reader is referred to the Web version of this article.)

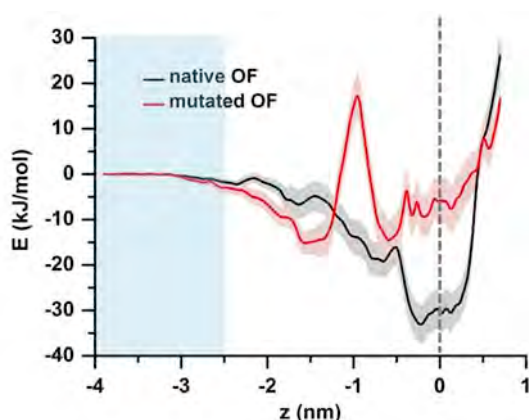


Fig. 7. Free energy profiles for the translocation of CYC across the native and mutated OF structures (mutation of Cys₃₂₇ to Ala).

would reduce the cellular protection from oxidative stress, as well as cancer cell drug resistance, eventually leading to cancer cell death. However, before the CYC uptake can be inhibited, we need to better understand the mechanism of CYC transport across the xCT antiporter at the molecular level. For this purpose, we constructed three model systems (i.e., the OF, OCC and IF structures) and we simulated the permeation of CYC across these systems, applying different simulation techniques. The accuracy of these model systems was verified using different programs and the structures of their channels were determined by calculation of their funnel radii. To find the CYC binding site in the OF, OCC and IF structures, we used SMD, TMD and conventional MD simulations. Analysis of the local (i.e., around the CYC binding site) and global conformational changes in these structures reveals the precise locations of the binding site, as well as the amino acid residues involved in this region, through calculation of the non-bonded energies between CYC and these residues. One of the important residues in the substrate binding site was found to be Arg₁₃₅ of the TM3 domain, which exhibits different binding energies with CYC, depending on the conformations of the xCT antiporter, having the strongest interaction in the case of the OF conformation. The free energy profiles of CYC across the OF, OCC and IF structures, calculated with US simulations, showed that the energy minimum of CYC is higher in the IF conformation. This indicates that a lower energy is required to release CYC from the antiporter. Finally, the effect of the mutation of Cys₃₂₇ to Ala in the OF structure was studied, by calculating the free energy profiles of the native and mutated OF structures, again with US simulations. We found that this mutation makes the CYC transportation

across the xCT antiporter more difficult, leading to a decrease of the CYC permeation rate. This is in qualitative agreement with experiments [48], where a drop of the CYC uptake by the xCT⁻ antiporter was observed upon this mutation. Our findings indicate that the chosen model systems are adequate and the obtained results support the experiments.

This study is important, since it elucidates the molecular level mechanisms of the CYC uptake by the xCT subunit of the xCT⁻ antiporter, which affects the intracellular oxidative stress. Hence, this insight might be highly relevant for new cancer therapy studies. This will be investigated in our future work.

Acknowledgements

M. Y. gratefully acknowledges financial support from the Research Foundation – Flanders (FWO), grant numbers 1200216N and 1200219N. The computational work was carried out using the Turing HPC infrastructure at the CalcUA core facility of the Universiteit Antwerpen, a division of the Flemish Supercomputer Center VSC, funded by the Hercules Foundation, the Flemish Government (department EWI) and the UA. Finally, we thank A. S. Mashayekh Esfehan and A. Mohseni for their important comments on the manuscript.

Appendix A. Supplementary data

Supplementary data to this article can be found online at <https://doi.org/10.1016/j.abb.2019.01.039>.

References

- [1] G. Khelashvili, H. Weinstein, Functional mechanisms of neurotransmitter transporters regulated by lipid-protein interactions of their terminal loops, *Biochim. Biophys. Acta Biomembr.* 1848 (9) (2015) 1765–1774.
- [2] R.J. Kathawala, P. Gupta, C.R. Ashby Jr., Z.-S. Chen, The modulation of ABC transporter-mediated multidrug resistance in cancer: a review of the past decade, *Drug Resist. Updates* 18 (2015) 1–17.
- [3] X. Zha, Z. Hu, S. Ji, F. Jin, K. Jiang, C. Li, P. Zhao, Z. Tu, X. Chen, L. Di, NFκB up-regulation of glucose transporter 3 is essential for hyperactive mammalian target of rapamycin-induced aerobic glycolysis and tumor growth, *Cancer Lett.* 359 (1) (2015) 97–106.
- [4] H. Milton, V. Reddy, D. Tamang, A. Västermark, The transporter classification database, *Nucleic Acids Res.* 42 (2014) 251–258.
- [5] E. Padan, H. Michel, NhaA: a unique structural fold of secondary active transporters, *Isr. J. Chem.* 55 (11–12) (2015) 1233–1239.
- [6] E.M. Quistgaard, C. Löw, F. Guettou, P. Nordlund, Understanding transport by the major facilitator superfamily (MFS): structures pave the way, *Nat. Rev. Mol. Cell Biol.* 17 (2) (2016) 123.
- [7] J. Chillarón, R. Roca, A. Valencia, A. Zorzano, M. Palacín, Heteromeric amino acid transporters: biochemistry, genetics, and physiology, *Am. J. Physiol. Renal. Physiol.* 281 (6) (2001) F995–F1018.
- [8] H. Gmünder, H.-P. Eck, B. Benninghoff, S. Roth, W. Dröge, Macrophages regulate

- intracellular glutathione levels of lymphocytes. Evidence for an immunoregulatory role of cysteine, *Cell. Immunol.* 129 (1) (1990) 32–46.
- [9] T.B. Levring, M. Kongsbak, A.K. Rode, A. Woetmann, N. Ødum, C.M. Bonefeld, C. Geisler, Human CD4+ T cells require exogenous cystine for glutathione and DNA synthesis, *Oncotarget* 6 (26) (2015) 21853.
- [10] G. Wu, Y.-Z. Fang, S. Yang, J.R. Lupton, N.D. Turner, Glutathione metabolism and its implications for health, *J. Nutr.* 134 (3) (2004) 489–492.
- [11] X. Yu, Y.C. Long, Crosstalk between cystine and glutathione is critical for the regulation of amino acid signaling pathways and ferroptosis, *Sci. Rep.* 6 (2016) 30033.
- [12] M. Lo, Y.Z. Wang, P.W. Gout, The x cystine/glutamate antiporter: a potential target for therapy of cancer and other diseases, *J. Cell. Physiol.* 215 (3) (2008) 593–602.
- [13] Y. Dun, B. Mysona, T. Van Ells, L. Amarnath, M.S. Ola, V. Ganapathy, S.B. Smith, Expression of the cystine-glutamate exchanger (x c⁻) in retinal ganglion cells and regulation by nitric oxide and oxidative stress, *Cell Tissue Res.* 324 (2) (2006) 189–202.
- [14] J. Lewerenz, S.J. Hewett, Y. Huang, M. Lambros, P.W. Gout, P.W. Kalivas, A. Massie, I. Smolders, A. Methner, M. Pergande, The cystine/glutamate antiporter system xc⁻ in health and disease: from molecular mechanisms to novel therapeutic opportunities, *Antioxidants Redox Signal.* 18 (5) (2013) 522–555.
- [15] A.L. Edinger, C.B. Thompson, Antigen-presenting cells control T cell proliferation by regulating amino acid availability, *Proc. Natl. Acad. Sci. Unit. States Am.* 99 (3) (2002) 1107–1109.
- [16] H. Sies, Glutathione and its role in cellular functions, *Free Radic. Biol. Med.* 27 (9–10) (1999) 916–921.
- [17] R.J. Bridges, N.R. Natale, S.A. Patel, System xc-cystine/glutamate antiporter: an update on molecular pharmacology and roles within the CNS, *Br. J. Pharmacol.* 165 (1) (2012) 20–34.
- [18] L. Slosky, N. BassiriRad, A. Symons-Liguori, B. Forte, L. Bui, T. Largent-Milnes, T. Vanderah, (277) The cystine-glutamate antiporter system xc⁻ drives tumor cell glutamate release and cancer-induced bone pain, *J. Pain* 16 (4) (2015) S45.
- [19] K. Linher-Melville, M. Nashed, R. Ungard, S. Haftchenary, P. Gunning, G. Singh, Abstract P3-03-13: Chronic Inhibition of Signal Transducer and Activator of Transcription 3/5 in Treatment-Resistant Human Breast Cancer Cell Subtypes: Convergence on the Reactive Oxygen species/SUMOylation Pathway and its Effects on xCT Expression and System xc-Activity, *AACR*, 2017.
- [20] P. Gout, Y. Kang, D. Buckley, N. Bruchovsky, A. Buckley, Increased cystine uptake capability associated with malignant progression of Nb2 lymphoma cells, *Leukemia* 11 (8) (1997) 1329.
- [21] J. Liu, L. Feng, E.M. Stone, J. Tyler, S.W. Rowlinson, M.J. Keating, P. Huang, Targeting chronic lymphocytic leukemia by interfering glutathione synthesis using a novel therapeutic enzyme cyst (e) inase (AEB3103), *AACR*, 2016.
- [22] K. Tsuchihashi, S. Okazaki, M. Ohmura, M. Ishikawa, O. Sampetean, N. Onishi, H. Wakimoto, M. Yoshikawa, R. Seishima, Y. Iwasaki, The EGF receptor promotes the malignant potential of glioma by regulating amino acid transport system xc⁻, *Cancer Res.* (2016) canres. 2121.2015.
- [23] S. Lanzardo, L. Conti, R. Rooke, R. Ruiu, N. Accart, E. Bolli, M. Arigoni, M. Macagno, G. Barrera, S. Pizzimenti, Immunotargeting of antigen xCT attenuates stem-like cell behavior and metastatic progression in breast cancer, *Cancer Res.* (2015) canres. 1208.2015.
- [24] L. Dai, Y. Cao, Y. Chen, C. Parsons, Z. Qin, Targeting xCT, a cystine-glutamate transporter induces apoptosis and tumor regression for KSHV/HIV-associated lymphoma, *J. Hematol. Oncol.* 7 (1) (2014) 30.
- [25] M.-z. Ma, G. Chen, P. Wang, W.-h. Lu, C.-f. Zhu, M. Song, J. Yang, S. Wen, R.-h. Xu, Y. Hu, xc⁻ inhibitor sulfasalazine sensitizes colorectal cancer to cisplatin by a GSH-dependent mechanism, *Cancer Lett.* 368 (1) (2015) 88–96.
- [26] L. Sleire, B. Skeie, I. Netland, H. Førde, E. Dodo, F. Selheim, L. Leiss, J. Heggdal, P. Pedersen, J. Wang, Drug repurposing: sulfasalazine sensitizes gliomas to gamma knife radiosurgery by blocking cystine uptake through system xc⁻, leading to glutathione depletion, *Oncogene* 34 (49) (2015) 5951.
- [27] J.-L. Roh, E.H. Kim, H. Jang, D. Shin, Aspirin plus sorafenib potentiates cisplatin cytotoxicity in resistant head and neck cancer cells through xCT inhibition, *Free Radic. Biol. Med.* 104 (2017) 1–9.
- [28] W. Wang, I. Kryczek, L. Dostál, H. Lin, L. Tan, L. Zhao, F. Lu, S. Wei, T. Maj, D. Peng, Effector T cells abrogate stroma-mediated chemoresistance in ovarian cancer, *Cell* 165 (5) (2016) 1092–1105.
- [29] D. Patel, P.S. Kharkar, M. Nandave, Emerging roles of system antiporter and its inhibition in CNS disorders, *Mol. Membr. Biol.* 32 (4) (2015) 89–116.
- [30] H. Sato, M. Tamba, T. Ishii, S. Bannai, Cloning and expression of a plasma membrane cystine/glutamate exchange transporter composed of two distinct proteins, *J. Biol. Chem.* 274 (17) (1999) 11455–11458.
- [31] F. Verrey, E.I. Closs, C.A. Wagner, M. Palacin, H. Endou, Y. Kanai, CATs and HATs: the SLC7 family of amino acid transporters, *Pflügers Archiv* 447 (5) (2004) 532–542.
- [32] D. Fotiadis, Y. Kanai, M. Palacin, The SLC3 and SLC7 families of amino acid transporters, *Mol. Aspect. Cryst.* 34 (2–3) (2013) 139–158.
- [33] M. Smyth, J. Martin, x ray crystallography, *Mol. Pathol.* 53 (1) (2000) 8.
- [34] M. Palacin, E. Errasti-Murugarren, A. Rosell, Heteromeric amino acid transporters. In search of the molecular bases of transport cycle mechanisms, *Biochem. Soc. Trans.* 44 (3) (2016) 745–752.
- [35] R. Rodriguez, G. China, N. Lopez, T. Pons, G. Vriend, Homology modeling, model and software evaluation: three related resources, *Bioinformatics (Oxford, England)* 14 (6) (1998) 523–528.
- [36] G. Ciccotti, M. Ferrario, C. Schuette, Molecular dynamics simulation, *Entropy* 16 (2014) 233.
- [37] P.L. Shaffer, A. Goehring, A. Shankaranarayanan, E. Gouaux, Structure and mechanism of a Na⁺-independent amino acid transporter, *Science* 325 (5943) (2009) 1010–1014.
- [38] Y. Shi, Common folds and transport mechanisms of secondary active transporters, *Annu. Rev. Biophys.* 42 (2013) 51–72.
- [39] X. Gao, L. Zhou, X. Jiao, F. Lu, C. Yan, X. Zeng, J. Wang, Y. Shi, Mechanism of substrate recognition and transport by an amino acid antiporter, *Nature* 463 (7282) (2010) 828.
- [40] J. Li, P.-C. Wen, M. Moradi, E. Tajkhorshid, Computational characterization of structural dynamics underlying function in active membrane transporters, *Curr. Opin. Struct. Biol.* 31 (2015) 96–105.
- [41] P. Ferrara, J. Apostolakis, A. Cafilisch, Targeted molecular dynamics simulations of protein unfolding, *J. Phys. Chem. B* 104 (18) (2000) 4511–4518.
- [42] J.S. Patel, A. Berteotti, S. Ronsisvalle, W. Rocchia, A. Cavalli, Steered molecular dynamics simulations for studying protein–ligand interaction in cyclin-dependent kinase 5, *J. Chem. Inf. Model.* 54 (2) (2014) 470–480.
- [43] K. Kappel, Y. Miao, J.A. McCammon, Accelerated molecular dynamics simulations of ligand binding to a muscarinic G-protein-coupled receptor, *Q. Rev. Biophys.* 48 (4) (2015) 479–487.
- [44] A.J. Clark, P. Tiwary, K. Borrelli, S. Feng, E.B. Miller, R. Abel, R.A. Friesner, B. Berne, Prediction of protein–ligand binding poses via a combination of induced fit docking and metadynamics simulations, *J. Chem. Theor. Comput.* 12 (6) (2016) 2990–2998.
- [45] J. Kästner, Umbrella sampling, *Wiley Interdiscip. Rev.: Comput. Mol. Sci.* 1 (6) (2011) 932–942.
- [46] M. Gur, E. Zomot, M.H. Cheng, I. Bahar, Energy landscape of LeuT from molecular simulations, *J. Chem. Phys.* 143 (24) (2015) 12B611_1.
- [47] H.D. Song, F. Zhu, Conformational changes in two inter-helical loops of Mhp1 membrane transporter, *PLoS One* 10 (7) (2015) e0133388.
- [48] M. Jiménez-Vidal, E. Gasol, A. Zorzano, V. Nunes, M. Palacin, J. Chillarón, Thiol modification of cysteine 327 in the eighth transmembrane domain of the light subunit xCT of the heteromeric cystine/glutamate antiporter suggests close proximity to the substrate binding site/permeation pathway, *J. Biol. Chem.* 279 (12) (2004) 11214–11221.
- [49] H. Berman, K. Henrick, H. Nakamura, Announcing the worldwide protein data bank, *Nat. Struct. Mol. Biol.* 10 (12) (2003) 980.
- [50] H. Nielsen, J. Engelbrecht, G. von Heijne, S. Brunak, Defining a similarity threshold for a functional protein sequence pattern: the signal peptide cleavage site, *Proteins: Struct. Funct. Bioinf.* 24 (2) (1996) 165–177.
- [51] L. Kowalczyk, M. Ratera, A. Paladino, P. Bartocconi, E. Errasti-Murugarren, E. Valencia, G. Portella, S. Bial, A. Zorzano, I. Fita, Molecular basis of substrate-induced permeation by an amino acid antiporter, *Proc. Natl. Acad. Sci. U. S. A.* 108 (10) (2011) 3935.
- [52] D. Ma, P. Lu, C. Yan, C. Fan, P. Yin, J. Wang, Y. Shi, Structure and mechanism of a glutamate–GABA antiporter, *Nature* 483 (7391) (2012) 632.
- [53] E. Gasol, M. Jiménez-Vidal, J. Chillarón, A. Zorzano, M. Palacin, Membrane topology of system xc-light subunit reveals a reentrant loop with substrate-restricted accessibility, *J. Biol. Chem.* 279 (30) (2004) 31228–31236.
- [54] A. Waterhouse, M. Bertoni, S. Bienert, G. Studer, G. Tauriello, R. Gumienny, F.T. Heer, T.A.P. de Beer, C. Rempfer, L. Bordoli, SWISS-MODEL: homology modelling of protein structures and complexes, *Nucleic Acids Res.* 46 (W1) (2 July 2018) W296–W303.
- [55] M.A. Lomize, I.D. Pogozheva, H. Joo, H.I. Mosberg, A.L. Lomize, OPM database and PPM web server: resources for positioning of proteins in membranes, *Nucleic Acids Res.* 40 (D1) (2011) D370–D376.
- [56] S. Jo, T. Kim, V.G. Iyer, W. Im, CHARMM-GUI: a web-based graphical user interface for CHARMM, *J. Comput. Chem.* 29 (11) (2008) 1859–1865.
- [57] E.L. Wu, X. Cheng, S. Jo, H. Rui, K.C. Song, E.M. Dávila-Contreras, Y. Qi, J. Lee, V. Monje-Galvan, R.M. Venable, CHARMM-GUI membrane builder toward realistic biological membrane simulations, *J. Comput. Chem.* 35 (27) (2014) 1997–2004.
- [58] S. Bannai, E. Kitamura, Role of proton dissociation in the transport of cystine and glutamate in human diploid fibroblasts in culture, *J. Biol. Chem.* 256 (11) (1981) 5770–5772.
- [59] D. van der Spoel, P.J. van Maaren, C. Caleman, GROMACS molecule & liquid database, *Bioinformatics* 28 (5) (2012) 752–753.
- [60] M.J. Frisch, G.W. Trucks, H.B. Schlegel, G.E. Scuseria, M.A. Robb, J.R. Cheeseman, G. Scalmani, V. Barone, G.A. Petersson, H. Nakatsuji, X. Li, M. Caricato, A.V. Marenich, J. Bloino, B.G. Janesko, R. Gomperts, B. Mennucci, H.P. Hratchian, J.V. Ortiz, A.F. Izmaylov, J.L. Sonnenberg, Williams, F. Ding, F. Lipparini, F. Egidi, J. Goings, B. Peng, A. Petrone, T. Henderson, D. Ranasinghe, V.G. Zakrzewski, J. Gao, N. Rega, G. Zheng, W. Liang, M. Hada, M. Ehara, K. Toyota, R. Fukuda, J. Hasegawa, M. Ishida, T. Nakajima, Y. Honda, O. Kitao, H. Nakai, T. Vreven, K. Throssell, J.A. Montgomery Jr., J.E. Peralta, F. Ogliaro, M.J. Bearpark, J.J. Heyd, E.N. Brothers, K.N. Kudin, V.N. Staroverov, T.A. Keith, R. Kobayashi, J. Normand, K. Raghavachari, A.P. Rendell, J.C. Burant, S.S. Iyengar, J. Tomasi, M. Cossi, J.M. Millam, M. Klene, C. Adamo, R. Cammi, J.W. Ochterski, R.L. Martin, K. Morokuma, O. Farkas, J.B. Foresman, D.J. Fox, *Gaussian 16 Rev. B.01*, (2016) Wallingford, CT.
- [61] K. Vanommeslaeghe, E. Hatcher, C. Acharya, S. Kundu, S. Zhong, J. Shim, E. Darian, O. Guvench, P. Lopes, I. Vorobyov, CHARMM general force field: a force field for drug-like molecules compatible with the CHARMM all-atom additive biological force fields, *J. Comput. Chem.* 31 (4) (2010) 671–690.
- [62] J. Pontius, J. Richelle, S.J. Wodak, Deviations from standard atomic volumes as a quality measure for protein crystal structures, *J. Mol. Biol.* 264 (1) (1996) 121–136.
- [63] J.C. Phillips, R. Braun, W. Wang, J. Gumbart, E. Tajkhorshid, E. Villa, C. Chipot, R.D. Skeel, L. Kale, K. Schulten, Scalable molecular dynamics with NAMD, *J. Comput. Chem.* 26 (16) (2005) 1781–1802.
- [64] J.B. Klauda, R.M. Venable, J.A. Freites, J.W. O'Connor, D.J. Tobias, C. Mondragon-

- Ramirez, I. Vorobyov, A.D. MacKerell Jr., R.W. Pastor, Update of the CHARMM all-atom additive force field for lipids: validation on six lipid types, *J. Phys. Chem. B* 114 (23) (2010) 7830–7843.
- [65] R.B. Best, X. Zhu, J. Shim, P.E. Lopes, J. Mittal, M. Feig, A.D. MacKerell Jr., Optimization of the additive CHARMM all-atom protein force field targeting improved sampling of the backbone ϕ , ψ and side-chain χ_1 and χ_2 dihedral angles, *J. Chem. Theor. Comput.* 8 (9) (2012) 3257–3273.
- [66] D.J. Evans, B.L. Holian, The nose–hoover thermostat, *J. Chem. Phys.* 83 (8) (1985) 4069–4074.
- [67] M. Parrinello, A. Rahman, Polymorphic transitions in single crystals: a new molecular dynamics method, *J. Appl. Phys.* 52 (12) (1981) 7182–7190.
- [68] O.S. Smart, J.G. Neduveilil, X. Wang, B. Wallace, M.S. Sansom, HOLE: a program for the analysis of the pore dimensions of ion channel structural models, *J. Mol. Graph.* 14 (6) (1996) 354–360.
- [69] W. Humphrey, A. Dalke, K. Schulten, VMD: visual molecular dynamics, *J. Mol. Graph.* 14 (1) (1996) 33–38.
- [70] S. Pronk, S. Páll, R. Schulz, P. Larsson, P. Bjelkmar, R. Apostolov, M.R. Shirts, J.C. Smith, P.M. Kasson, D. Van Der Spoel, GROMACS 4.5: a high-throughput and highly parallel open source molecular simulation toolkit, *Bioinformatics* 29 (7) (2013) 845–854.
- [71] M.J. Abraham, T. Murtola, R. Schulz, S. Páll, J.C. Smith, B. Hess, E. Lindahl, GROMACS: high performance molecular simulations through multi-level parallelism from laptops to supercomputers, *SoftwareX* 1 (2015) 19–25.
- [72] W.L. DeLano, *The PyMOL Molecular Graphics System*, (2002) <http://www.pymol.org>.
- [73] J.S. Hub, B.L. De Groot, D. Van Der Spoel, g_wham – a free weighted histogram analysis implementation including robust error and autocorrelation estimates, *J. Chem. Theor. Comput.* 6 (12) (2010) 3713–3720.
- [74] R. Dubey, *A Textbook of Biotechnology*, S. Chand Publishing, 1993.